

Phenylcarbazole-dipyridyl triazole hybrid as bipolar host material for phosphorescent OLEDs

Wen-Yi Hung,^{*a} Guan-Min Tu,^b Shou-Wei Chen^a and Yun Chi^{*b}

Received 17th November 2011, Accepted 6th January 2012

DOI: 10.1039/c2jm15963e

Two bipolar host materials p-cbtz and m-cbtz, with both phenylcarbazole and 3,5-bis(2-pyridyl)-1,2,4-triazole moieties, were synthesized and tested for fabrication of various phosphorescent OLEDs. The sp³-hybridized nitrogen atom of the 1,2,4-triazole fragment disrupted the π -conjugation between the electron donating 9-phenylcarbazole and the electron accepting 3,5-bis(2-pyridyl)-1,2,4-triazole and, thus, exhibited promising properties such as bipolar charge transport feature (10^{-5} – 10^{-6} cm² V⁻¹s⁻¹) and with relatively high triplet energy gaps ($E_T = 2.82$ – 2.75 eV). As a result, they were utilized as universal hosts for various phosphorescent OLEDs, showing high efficiencies and low efficiency roll-off. For example, the devices hosted by m-cbtz achieve maximum external quantum efficiencies (η_{ext}) of 8.8% for blue, 16.7% for green, 17.5% for yellow and 16.7% for red-emitting OLEDs. In addition, we also fabricated dual-emitter WOLEDs with a co-doped single emissive layer, exhibiting satisfactory device efficiencies (12.4%, 25 cd A⁻¹, 17 lm W⁻¹) and with highly stable chromaticity (CIE_x = 0.26–0.27 and CIE_y = 0.38) at an applied voltage of 8 to 11 V. These results demonstrated that the newly synthesized, phenylcarbazole-dipyridyl triazole host materials are advantageous for fabrication of various highly efficient phosphorescent OLEDs.

Introduction

Phosphorescent organic light-emitting diodes (PhOLEDs) have high potential for fabrication of next generation full color displays and solid-state lighting due to the low manufacturing cost and excellent versatility to adopt various applications. In addition, in contrast to the typical fluorescent OLEDs, the phosphorescent (Ph) OLEDs can reach to 100% of theoretical internal quantum efficiency by harvesting both singlet and triplet excitons.¹ In order to maximize the actual efficiency and to reduce concentration quenching (triplet–triplet annihilation) of PhOLEDs, the host–guest strategy is implemented by dispersing (or doping) the metal based phosphors (guests) homogeneously into a suitable organic matrix (host) to suppress this detrimental effect. The host material serves as the platform for holes and electrons recombination to form excitons, as well as for both singlet-to-singlet and triplet-to-triplet excitation energy transfer from host to dopant. Hence, the triplet energies of the host material should be higher than that of the phosphor to confine the as-generated excitons within the emissive layer. In addition, host materials with good carrier transporting properties are

required to increase the electrons and holes recombination within the emissive layer.

To cope with this demand, recent research trends have shifted to the development of host materials possessing bipolar properties.² It is believed that, upon incorporating both the electron-donating (D) and electron-accepting (A) moieties into the single molecule, the resulting bipolar host materials are then able to perform balanced injection/transportation/recombination of charge carriers and, consequentially, to give OLEDs with higher performance characteristics and lower efficiency roll-off. However, the co-existence of these D and A groups may also lead to an unwanted, intramolecular charge transfer, resulting in severe reduction of the triplet energy of the host. To suppress the intramolecular charge transfer, the electronic coupling between D and A moieties must be reduced by a certain linker featured with a twisted π -conformation, *i.e.* connecting the D and A units through *meta*- and/or *ortho*-linkages instead of the *para*-position on the hexagonal aromatic fragment.³ The incorporation of saturated atomic linkages, such as sp³-hybridized atoms⁴ or non-conjugated σ -linkages,⁵ serve as an alternative to suppress direct interactions between the D and A moieties.

From the material perspective, phenylcarbazole and/or triphenylamine derivatives have been widely used as host materials in PhOLEDs due to their sufficiently large triplet energies and good hole-transporting ability. Thus, addition of electron-transporting moieties into the above mentioned phenylcarbazole or triphenylamine derivatives became a generalized strategy for

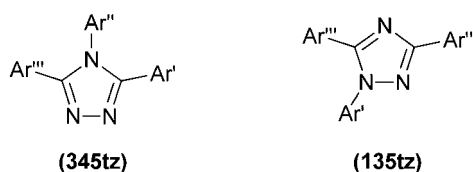
^aInstitute of Optoelectronic Sciences, National Taiwan Ocean University, Keelung, 202, Taiwan. E-mail: wenhung@mail.ntou.edu.tw; Fax: +886 2 24634360; Tel: +886 2 24622192 ext. 6718

^bDepartment of Chemistry, National Tsing Hua University, Hsinchu, 300, Taiwan. E-mail: ychi@mx.nthu.edu.tw; Fax: +886 3 5720864; Tel: +886 3 5712956

making the demanded bipolar host materials. For example, Sapochak *et al.* reported the incorporation of carbazole *via* a non-conjugated N-linkage to the peripheral phenylene ring of an n-type triphenylphosphine oxide (tPPO), giving the bipolar host known as *N*-(4-diphenylphosphorylphenyl)carbazole (MPO12).⁶ With FIrpic as the emitter, an MPO12-hosted OLED exhibits a maximum external quantum efficiency of 7.1%. Guan *et al.* reported the successful preparation of three carbazole/oxadiazole derivatives, by linking the carbazole and oxadiazole with the non-conjugated methylene spacer.^{5a} The resulting bipolar host materials t-CmOxa were then successfully used in making red-emitting OLEDs with maximum external quantum efficiency and power efficiency of 9.5% and 9.9 lm W⁻¹. Lin *et al.* reported a benzimidazole/carbazole hybrid with a biphenyl bridge, which was then successfully used as a host for a single-layer Ir(ppy)₃ based OLED with maximum current and external quantum efficiencies of 34.3 cd A⁻¹ and 9.3%.⁷ Kim *et al.* documented a series of bipolar hosts comprising 1,2,4-triazole (TAZ) and 9-phenylcarbazole (Cz-Ph) for blue-emitting PhOLEDs.⁸ Yang *et al.* designed and synthesized a series of 1,2,4-triazole-cored triphenylamine derivatives as bipolar host materials, the maximum external quantum efficiencies reached 16.4% for red phosphorescence, and 14.2% for green-emitting OLEDs.^{3d} According to these literature reports,^{3d,8} we concluded that, when the aryl functional groups connect to the 1,2,4-triazole core, the severe twisting between 1,2,4-triazole and all aryl groups has disrupted the π -conjugation, giving higher triplet energy and then making the host materials more tolerable for PhOLEDs.

In this study we decided to circumvent the typical molecular design for the 3,4,5-trisubstituted 1,2,4-triazole hybrids and focus only on the 3,5-bis(2-pyridyl)-1*H*-1,2,4-triazole derived bipolar hosts with either *para*- or *meta*-substituted 9-phenylcarbazole fragment located at the N-1 position, *i.e.* affording the distinctive 1,3,5-trisubstituted 1,2,4-triazole core geometry. To the best of our knowledge, although 3,4,5-trisubstituted 1,2,4-triazoles (345tz) functionalities were widely used as the materials for organic photoelectronic applications,^{3d,8,9} there is no precedent for 1,3,5-trisubstituted 1,2,4-triazole (135tz) as a host of emissive layer or even electron-transport materials (Scheme 1).

Naturally, we expect that different linking topologies of the 9-phenylcarbazole and 3,5-bis(2-pyridyl)-1*H*-1,2,4-triazole would allow fine-tuning of their photophysical properties, better modulation of their triplet gaps, adequate HOMO/LUMO separations and charge balance, and eventually making them the universal design for hosts used in multicolor phosphorescent OLEDs. The OLED devices fabricated using m-cbtz have achieved maximum external quantum efficiency of 8.8%, 16.7%, 17.5% and 16.7% for blue (FIrpic), green [(ppy)₂Ir(acac)], yellow [(Bt)₂Ir(acac)], and red [Os(bpftz)₂(PPhMe₂)₂], respectively.



Scheme 1 Generalized structural drawing of 1,3,5-trisubstituted (135tz) and 3,4,5-trisubstituted 1,2,4-triazoles (345tz).

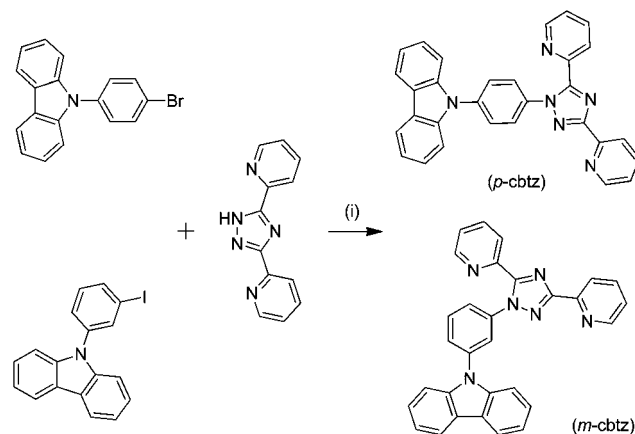
Finally, mimicking the rapid developments in WOLED research,¹⁰ two-emitter white OLEDs with co-doped single emissive layer were also examined, exhibiting efficiency of 12.4% and high chromatic stability (CIE_x = 0.26–0.27 and CIE_y = 0.38) at an applied voltage of 8 to 11 V.

Results and discussion

Two substituted 9-phenylcarbazole compounds, for which the halide substituent on the phenyl fragment is located at either the *para*- or *meta*-position *versus* the unique nitrogen atom, were synthesized using the Ullmann coupling reaction.¹¹ After then, the desired host materials p-cbtz and m-cbtz were synthesized by a second C–N bond coupling between the aforementioned phenylcarbazole and 3,5-bis(2-pyridyl)-1*H*-1,2,4-triazole in the presence of CuI catalyst (Scheme 2). Both materials were obtained as white powders in good yields and were purified by both recrystallization and vacuum sublimation before spectral characterization and device fabrication. In contrast, the phenylene linker of p-cbtz and m-cbtz is located at the N-1 nitrogen atom, rather than the N-4 nitrogen atom of the triazole fragment, the latter is typical for triazole based host materials.^{3d,8,9} Such a molecular arrangement is controlled by their synthetic approach and, theoretically, could afford host materials with different physical properties.

Their physical properties were investigated by thermogravimetric analysis (TGA) and differential scanning calorimetry (DSC) in Table 1. In the TGA measurements, both p-cbtz and m-cbtz exhibited high decomposition temperatures (T_d , corresponding to 5% weight loss) at 358 and 331 °C, respectively. The *para*-substituted p-cbtz appears to have a higher T_g value of 86 °C than its congener with *meta*-substituted derivative (m-cbtz, T_g = 77 °C), which can be rationalized by the greater disorder in energy.¹²

Fig. 1 displays UV–Vis absorption and photoluminescence (PL) spectra (recorded at room temperature) of p-cbtz and m-cbtz in 2-MeTHF solution (10⁻⁵ M) and in the form of solid thin film, as well as their phosphorescence spectra in 2-MeTHF solution (10⁻⁵ M) at 77 K (see Table 1). Apparently, the introduction of different linking topologies on 9-phenylcarbazole and 3,5-bis(2-pyridyl)-1,2,4-triazole only brings out limited



Scheme 2 Synthetic route to the host materials p-cbtz and m-cbtz; conditions: (i), CuI, K₂CO₃, DMF, reflux, 36 h.

Table 1 Physical properties of p-cbtz and m-cbtz

	$(T_g/T_c/T_m)/^{\circ}C$	$T_d/^{\circ}C$	${}^a E_{1/2}^{ox}/V$	(HOMO/LUMO/ E_g) ^b /eV	E_T ^c /eV	λ_{abs}/nm [sol./film]	λ_{pl}/nm [sol./film]	$(\mu_h/\mu_e)^d/cm^2 V^{-1} s^{-1}$
p-cbtz	86/—/215	358	0.99	−5.69/−2.12/3.57	2.82	291, 323, 339/285, 330, 344	427/425	$1.3 \times 10^{-5}/2.6 \times 10^{-6}$
m-cbtz	77/134/233	331	0.97	−5.68/−2.15/3.53	2.75	293, 325, 340/286, 329, 342	427/422	$8.7 \times 10^{-6}/1.1 \times 10^{-6}$

^a Oxidation potential was measured using cyclic voltammetry (CV) in CH_2Cl_2 solution. ^b HOMO was determined by AC-2 measurements, while LUMO was calculated using the equation $LUMO = HOMO + E_g$, where E_g was extracted from the absorption onset of solid film. ^c E_T was measured in 2-MeTHF at 77 K with a sample concentration of 10^{-5} M and an excitation wavelength of 338 nm. ^d μ was determined from the TOF measurement at $E = 9.0 \times 10^5$ V cm^{-1} .

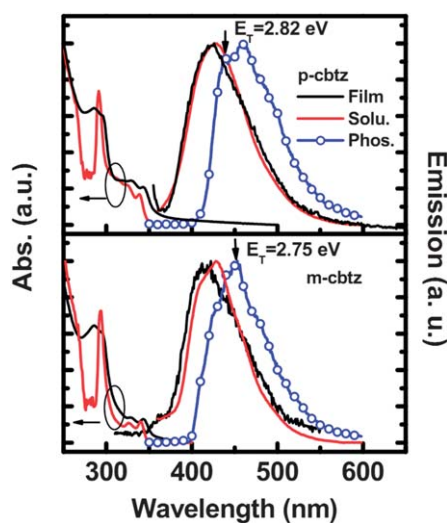


Fig. 1 Room-temperature UV-Vis absorption and PL spectra of p-cbtz and m-cbtz in 2-MeTHF solution (10^{-5} M) and as neat film, as well as the corresponding solution phosphorescence recorded at 77 K.

perturbation of the photophysical properties. A strong absorption peak at *ca.* 290 nm and two weak absorption peaks at *ca.* 325 and 340 nm are attributed to the π - π^* and n - π^* transitions of the 9-phenylcarbazole. In addition, no charge transfer absorption band from the electron-donating 9-phenylcarbazole to the electron-withdrawing 3,5-bis(2-pyridyl)-1,2,4-triazole can be observed,⁸ indicating the disruption of the π -conjugation between these parts owing to the connection at the sp^3 -hybridized nitrogen atom. The emission spectra in solution and as neat film are also similar, both giving peak patterns at *ca.* 422–427 nm. The triplet energies of p-cbtz and m-cbtz were determined to be 2.82 and 2.75 eV by the highest energy 0–0 phosphorescence, which are sufficiently higher than that of blue phosphor (FlRpic, $E_T = 2.65$ eV)¹³ and all other long-wavelength phosphors, implying effective confinement of the triplet excitons in the emissive layer and blockage of back energy transfer from the guest to the host.

The electrochemical properties of p-cbtz and m-cbtz were investigated by cyclic voltammetry (CV). After that, we used a photoemission spectrometer (Riken AC-2) to determine the HOMO energy levels of p-cbtz and m-cbtz, while their LUMO energy levels were estimated from the HOMO energy level and the optical band gaps (E_g) using the equation $LUMO = HOMO + E_g$. Table 1 also summarizes the HOMO and LUMO energy levels. The HOMOs span a narrow range of 5.68–5.69 eV,

but the LUMO of p-cbtz (2.12 eV) is slightly higher than that of m-cbtz (2.15 eV), which could be attributed to the distinctive bonding mode of the phenylene linker.

In order to confirm this hypothesis that the appending of the electron-donating 9-phenylcarbazole onto the electron-withdrawing 3,5-bis(2-pyridyl)-1,2,4-triazole renders p-cbtz and m-cbtz with promising bipolar transporting properties, we used time-of-flight (TOF) techniques to measure the associated carrier mobility.¹⁴ The device used for TOF measurement was prepared through vacuum deposition of the tri-layer structure ITO glass/p-cbtz (1.11 μm) or m-cbtz (1.51 μm)/Ag (150 nm), followed by placing them inside a vacuum chamber for data measurement. Fig. 2(a)–(d) display typical room-temperature TOF transients for these materials under an applied electric field, for which we observe dispersive transient photocurrents from both holes and electrons. Using double-logarithmic representations [insets to Fig. 2(a)–(d)], we extracted the carrier-transit times (t_T), which are required to determine the carrier mobilities, from the intersections of the two asymptotes. We then calculated the mobility using the formula $\mu = d^2/Vt_T$, where d is the sample thickness and V is the applied voltage. Fig. 3 shows the carrier mobilities of p-cbtz and m-cbtz plotted as a function of the square root of the applied electric field, as well as the nearly universal Poole–Frenkel relationship. The hole mobilities fell within the range from 2.8×10^{-6} to 1.4×10^{-5} $cm^2 V^{-1} s^{-1}$ for fields varying from 3.6×10^5 to 1×10^6 V cm^{-1} , which are higher than the electron

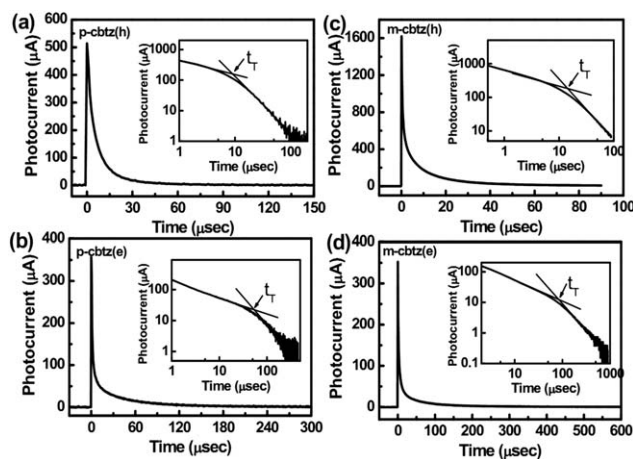


Fig. 2 Transient photocurrent signals for p-cbtz (1.11 μm thick) at $E = 8.98 \times 10^5$ V cm^{-1} and m-cbtz (1.51 μm thick) at $E = 1.06 \times 10^6$ V cm^{-1} : (a) (c) holes; (b) (d) electrons. Insets are the double logarithmic plots.

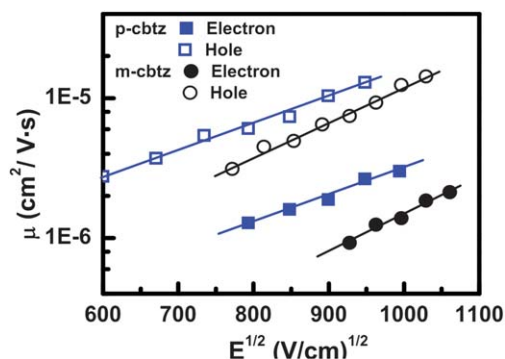
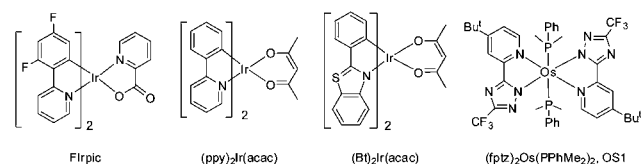


Fig. 3 Electron and hole mobilities versus $E^{1/2}$ for p-cbtz and m-cbtz.

mobilities: within the range from 9.2×10^{-7} to 3×10^{-6} $\text{cm}^2 \text{V}^{-1} \text{s}^{-1}$ for fields varying from 6.3×10^5 to 1.1×10^6 V cm^{-1} . The values of the carrier mobilities in both compounds at 9.0×10^5 V cm^{-1} are given in Table 1. Interestingly, the hole- and electron-mobilities of p-cbtz are *ca.* two-times greater than those of m-cbtz. This can be attributed to the fact that the *meta*-linkage may possess a greater degree of twisted conformation versus the corresponding *para*-conformation and, consequently, larger molecular disorders, which may impede the carrier hopping among the adjacent molecules.¹⁵

To evaluate the practical utility of p-cbtz and m-cbtz as host materials, we fabricated PhOLED devices with four phosphors, namely: [bis(4,6-difluorophenyl)-pyridinato-*N,C*']iridium(III) picolinate (FIrpic),¹⁶ bis(2-phenylpyridinato)iridium(III)(acetylacetonate) [(ppy)₂Ir(acac)],¹⁷ bis(2-phenylbenzothiazolato)iridium(III)(acetylacetonate) [(Bt)₂Ir(acac)],¹⁸ and bis[3-(trifluoromethyl)-5-(4-*tert*-butylpyridyl)-1,2,4-triazolate]osmium(II)bis(dimethylphenylphosphine) [Os(bpftz)₂(PPhMe₂)₂, OS1]¹⁹ (Scheme 3). To improve the hole injection from the anode, poly(3,4-ethylene-dioxythiophene): poly(styrene sulfonic acid) (PEDOT:PSS) was spun onto the precleaned ITO substrate to form a 30 nm-thick polymer buffer layer. Two hole transport layers (HTLs), which consisted of a 20 nm-thick layer of 4,4'-bis[*N*-(1-naphthyl)-*N*-phenyl]biphenyldiamine (NPB)²⁰ and a 5 nm-thick thick layer of 4,4',4'-tri(*N*-carbazolyl)triphenylamine (TCTA)²¹ were implemented. It is notable that TCTA with $E_T = 2.76$ eV and HOMO/LUMO levels of 5.7/2.4 eV also served as the triplet blocker to confine the excitons in the emissive layer. Moreover, a 25 nm-thick emissive layer consists of 10 wt.% of phosphors doped into the host material. For the blue device, electron transport layers (ETLs) consisted of a 5 nm-thick layer of diphenyl-bis[4-(pyridin-3-yl)phenyl]silane (DPPS),²² and a 45 nm-thick layer of 3-(4-biphenyl)-4-phenyl-5-(4-*tert*-butylphenyl)-1,2,4-triazole (TAZ),²³ for which DPPS ($E_T = 2.7$ eV, HOMO/LUMO = 6.5/2.5 eV) can be more effectively in blocking



Scheme 3 Chemical structures of the four dopants used in this study.

the excitons within the emissive layer, owing to the greater triplet energy gap than that of TAZ.²⁴ For other devices, a 50 nm-thick layer of 1,3,5-tris(*N*-phenylbenzimidazol-2-yl)benzene (TPBI) was used as the ETL instead of DPPS/TAZ (in blue-emitting OLEDs) for enhancement of electron injection. A cathode consisting of a 0.5 nm-thick layer of LiF and a 100 nm-thick layer of Al were deposited through a shadow mask.

Fig. 4 and 5 depict the current density–voltage–luminance (J – V – L) characteristics, device efficiencies, and EL spectra of the devices incorporating p-cbtz and m-cbtz host materials, respectively. Table 2 summarizes the electroluminescence data obtained. For all phosphorescent OLEDs, the higher efficiency was achieved for the m-cbtz based devices. The blue emission device **B2** reveals a maximum brightness of 29500 cd m^{-2} at 13.5 V (690 mA cm^{-2}) with the CIE coordinates of (0.16, 0.34). The maximum external quantum (η_{ext}), current (η_c), and power efficiencies (η_p) were 8.8%, 18 cd A^{-1} , and 9.8 lm W^{-1} , respectively.

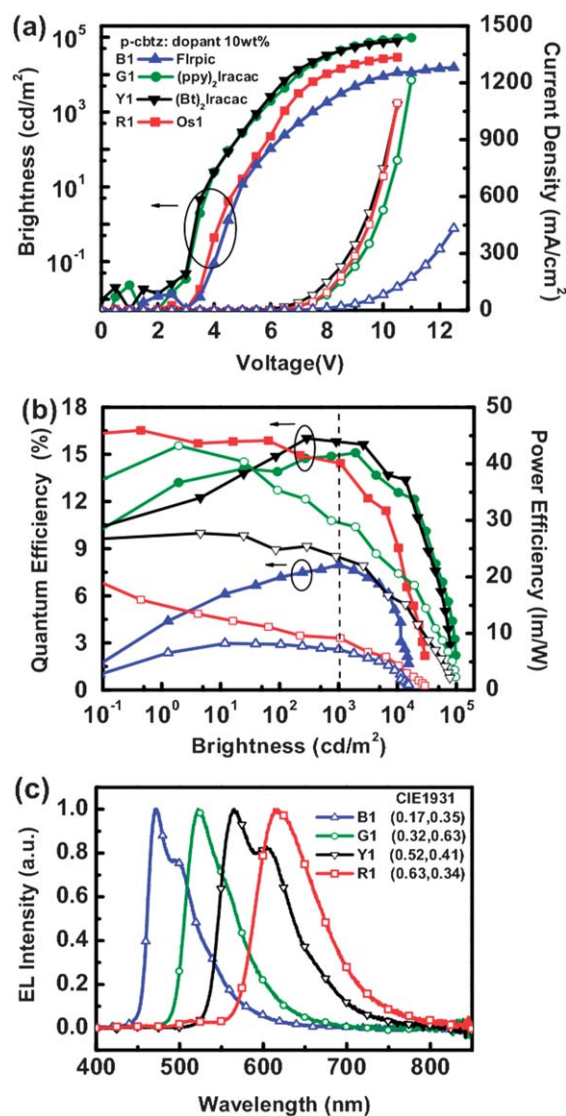


Fig. 4 (a) Current density–voltage–luminance (J – V – L) characteristics, (b) external quantum (η_{ext}) and power efficiencies (η_p) as a function of brightness, and (c) EL spectra for devices incorporating p-cbtz.

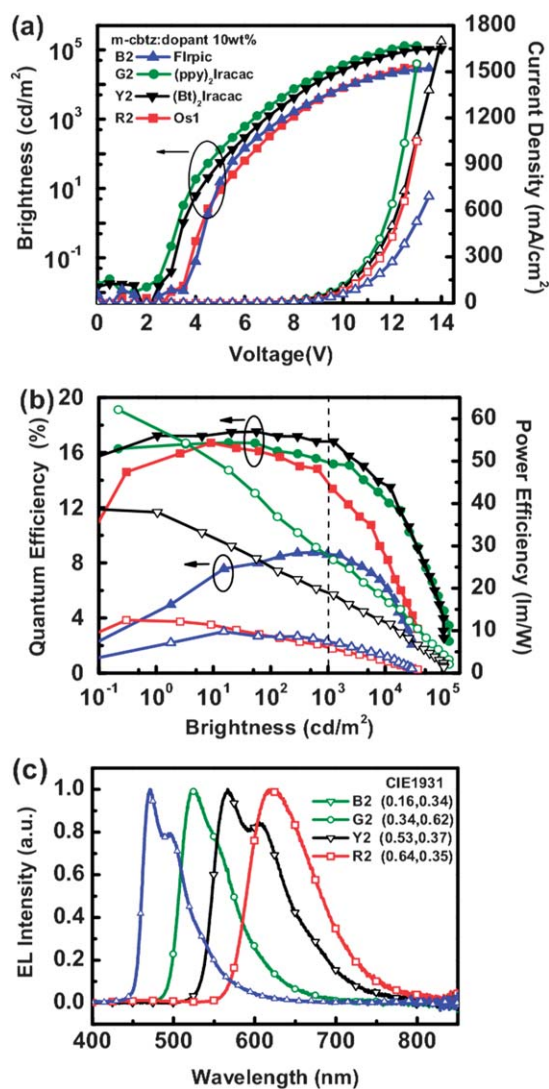


Fig. 5 (a) Current density–voltage–luminance (J – V – L) characteristics, (b) external quantum (η_{ext}) and power efficiencies (η_p) as a function of brightness, and (c) EL spectra for devices incorporating m-cbtz as host.

In comparison, lower efficiencies of 8%, 17.1 cd A⁻¹, and 8.2 lm W⁻¹ were obtained for the p-cbtz based device **B1**. The EL spectra of FIrpic-based devices are shown in Fig. 4(c) and 5(c).

Table 2 EL performances of devices

Dopant (10 wt.%)	V_{on}^b/V	$L_{\text{max}}/\text{cd m}^{-2}$	$I_{\text{max}}/\text{mA cm}^{-2}$	$\eta_{\text{ext}}^c/\%$	$\eta/\text{cd A}^{-1}$	$\eta_p/\text{lm W}^{-1}$	η_{ext} at 10 ³ cd m ^{-2c} /%	
B1 ^a	FIrpic	3.5	15500 (12.5 V)	430	8	17.1	8.2	8.0 (7.5V)
G1	(ppy) ₂ Ir(acac)	3.0	97100 (11 V)	1210	15.1	55	43	14.9 (5.6V)
Y1	(Bt) ₂ Ir(acac)	3.0	78000 (10.5 V)	1080	16	40.4	27.7	15.8 (5.5V)
R1	Os(bpftz) ₂ (PPhMe ₂) ₂ , OS1	3.5	29100 (10.5 V)	1090	16.5	20.3	18.8	14.4 (6.5V)
W1	FIrpic + 0.3% OS1	3.5	21200 (11.5 V)	640	9.1	17.9	11	9.0 (6.7V)
B2	FIrpic	3.5	29500 (13.5 V)	690	8.8	18	9.8	8.8 (7.5V)
G2	(ppy) ₂ Ir(acac)	2.5	130800 (13 V)	1550	16.7	61	62	15.3 (6.2V)
Y2	(Bt) ₂ Ir(acac)	3.0	106000 (14 V)	1700	17.5	43	38	16.8 (6.8V)
R2	Os(bpftz) ₂ (PPhMe ₂) ₂ , OS1	3.5	36700 (13 V)	1050	16.7	18.2	12.5	13.5 (7.9V)
W2	FIrpic + 0.3% OS1	3.5	51000 (13.5 V)	1000	12.4	25	17	12.1 (7.3V)

^a The notation 1 and 2 indicates the devices fabricated with host materials p-cbtz and m-cbtz, respectively. ^b Turn-on voltage at which emission became detectable. ^c The values of driving voltage and η_{ext} of device at 1000 cd m⁻² are depicted in parentheses.

Both devices show the same main peak at 475 nm with a shoulder peak at 500 nm, arising from the typical emission of the phosphor FIrpic. These device performances are moderate among FIrpic-based OLEDs presumably because the E_T s of p-cbtz and m-cbtz are not sufficiently high ensuring efficient energy transfer from the host to the phosphor and triplet exciton confinement on the phosphor. Another reason for deferred device performance is that we chose TCTA as the exciton blocker to prevent exciton diffusion to the hole transporting layer, because the E_T of TCTA is not large enough to effectively prevent diffusion of blue excitons.²⁵ However, this is a worthy sacrifice to acquire a compromise among the E_T s of RGB phosphors.

To further evaluate the suitability of p-cbtz and m-cbtz for low energy triplet emitters, we fabricated green, yellow, and red-emitting devices, for which the device performances are all better than those obtained for blue OLEDs. Generally speaking, these devices have similar architecture as the aforementioned blue devices except for using TPBI as the ETL to facilitate electron injection and transport. Fig. 4(a) and 5(a) depict the J – V plots and other essential characteristics of the devices featuring TPBI as ETL. They exhibited turn-on voltages of 2.5–3.5 V (defined as the voltage at which EL became detectable) because of the variation of HOMO energy level of dopants. The devices hosted by p-cbtz exhibited significantly higher current density than those with m-cbtz. We attribute the enhanced device current when using p-cbtz as the host material, as revealed by its relatively high carrier transporting properties. In green phosphorescent devices (device **G1** and **G2**) using (ppy)₂Ir(acac) as dopant, hosts p-cbtz and m-cbtz have stronger influence on the charge transport, such that the driving voltage is approximately 5.6 and 6.5 V at 1000 cd m⁻², respectively. Particularly, the device **G2** exhibited a relatively high brightness of 130800 cd m⁻² at a current density of 1550 mA cm⁻² (13 V). In addition, the device **G2** incorporating m-cbtz host exhibited higher efficiencies (16.7%, 61 cd A⁻¹, and 62 lm W⁻¹) relative to those of device **G1** (15.1%, 55 cd A⁻¹, and 43 lm W⁻¹); these devices achieved better performances for blue electrophosphorescence. The decreased driving voltage of **G1** can be attributed to high hole- and electron-mobility of p-cbtz. However, the efficiency of the device based on p-cbtz is lower than that based on m-cbtz, which maybe due to the inferior carrier balance that caused a greater degree of triplet exciton quenching in the emissive layer. The same trend can be observed for devices with different dopants.

Next, the yellow-emitting OLEDs were fabricated using $(\text{Bt})_2\text{Ir}(\text{acac})$ as dopant. Excellent performance of yellow electrophosphorescence can be achieved for devices **Y1** and **Y2** (Table 2). Device **Y2** hosted by m-cbtz displays substantially higher efficiencies (17.5%, 43 cd A^{-1} , and 38 lm W^{-1}) than device **Y1** hosted by m-cbtz (16%, 40.4 cd A^{-1} , and 27.7 lm W^{-1}). Remarkably, device **Y2** shows rather low efficiency roll-off at a brightness of 1000 cd m^{-2} , while the recorded η_{ext} is still maintained as high as 16.8%. These values are comparable to those of the best yellow phosphorescent OLEDs in the literature,²⁶ which may serve as the potential emitting element for generating white emission in combination with a complementary blue phosphor.²⁷ Finally, we demonstrated red-emitting OLEDs using the emitter Os1 (devices **R1** and **R2**). Both devices also exhibit high performance. For instance, the device **R1** exhibited a maximum brightness of 29100 cd m^{-2} at 10.5 V and respectable EL efficiencies (16.5%, 20.3 cd A^{-1} , and 18.8 lm W^{-1}) with the CIE coordinates of (0.63, 0.34) while the device **R2** exhibited a maximum brightness of 36700 cd m^{-2} at 13 V and very good EL efficiencies (16.7%, 18.2 cd A^{-1} , and 12.5 lm W^{-1}) with the CIE coordinates of (0.64, 0.35). The devices displayed relatively pure red emission and there is no residual emission from the host and/or adjacent layers in Fig. 4(c) and 5(c), indicating that the electroluminescence is solely originated from the Os(II) dopant and with completed energy transfer from host to dopant. More importantly, the excellent performances, disregarding their emission hue, were obtained from the essentially identical architecture and incorporation of different phosphors, which make them very attractive for commercial applications of full-color displays.

In addition to the evaluation for multi-color phosphors, we also fabricated two-emitter WOLEDs (device **W1** and **W2**) by utilization of 10 wt.% FIrpic and 0.3 wt.% Os1 co-doped into either p-cbtz or m-cbtz to form a single emissive layer. The proportion of Os1 required to produce balanced white emission in these devices is relatively low because the red emission occurred from the combined effects of efficient energy transfer from the blue phosphor and exciton formation by direct charge trapping on Os1 dopant.²⁸ Fig. 6 shows the J - V - L characteristics and curves of external quantum efficiency and power efficiency versus brightness. Device **W1** with p-cbtz as host achieved a turn-on voltage of 3.5 V and a maximum brightness of 21200 cd m^{-2} (640 mA cm^{-2}) at 11.5 V. The maximum values were 9.1%, 17.9 cd A^{-1} and 11 lm W^{-1} for η_{ext} , η_{c} , and η_{p} , respectively. In comparison, device **W2** using m-cbtz as the host exhibited higher performance with even better efficiencies (η_{ext} , η_{c} , and η_{p}) of 12.4%, 25 cd A^{-1} , and 17 lm W^{-1} , respectively. Both devices **W1** and **W2** exhibit a significantly reduced efficiency roll-off: η_{ext} is still as high as 9% for **W1**, and 12.1% for **W2** at 1000 cd m^{-2} . Moreover, the WOLEDs showed excellent chromatic stability as shown in Fig. 7. When the voltage increases from 8 to 11 V, the Commission Internationale de L'Eclairage (CIE) coordinates varied only slightly from (0.29, 0.38) to (0.27, 0.37) for device **W1**, and from (0.27, 0.38) to (0.26, 0.38) for device **W2**. This could be attributed to the use of the bipolar host which may result in balanced charge fluxes and a broad distribution of recombination regions within the emissive layer. As a result, the recombination ratio in emissive layer was maintained

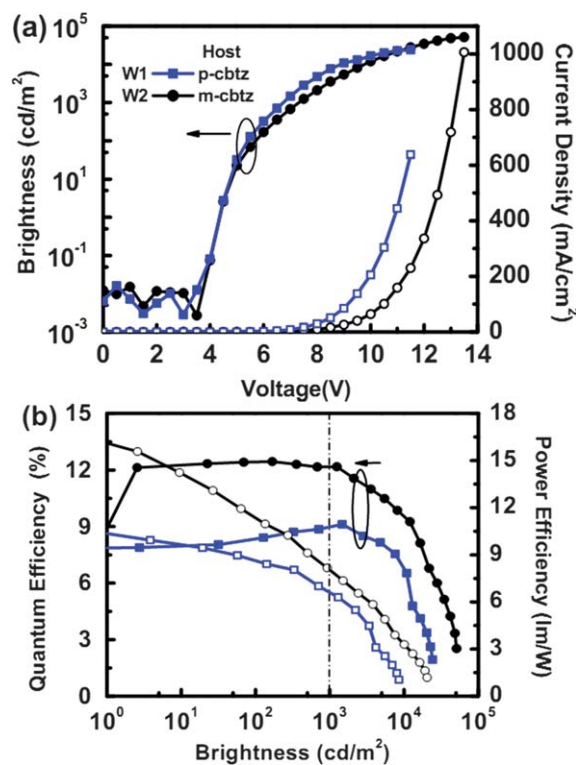


Fig. 6 (a) J - V - L characteristics, (b) plots of EL efficiency versus brightness for white devices under different hosts.

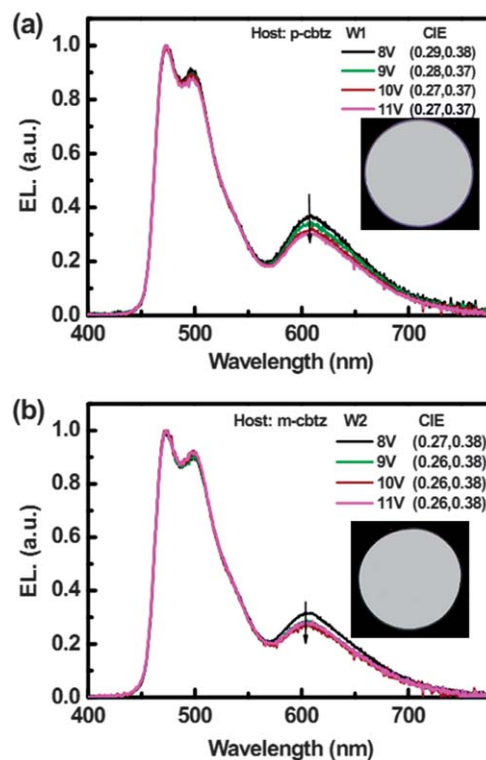


Fig. 7 The normalized EL spectra of white OLEDs employing (a) p-cbtz and (b) m-cbtz as host at various voltages.

invariant with increasing driving voltage, so as to keep the CIE coordinates almost constant.

Conclusions

We have synthesized and characterized two bipolar host materials, for which the phenylcarbazole and 3,5-bis(2-pyridyl)-1*H*-1,2,4-triazole fragments are linked with either *para*- or *meta*-phenyl bridging units. Furthermore, the relationship between their molecular structures and thermal, electrochemical and photophysical properties was addressed, and the influence of the host materials on the performances of phosphorescent OLEDs has been studied. Apparently, the introduction of different linking topologies (*para*- and *meta*-) only brings about limited perturbation of the photophysical properties. But, the hole and electron mobility of p-cbtz are *ca.* two-times higher than those of m-cbtz, which is attributed to the *meta*-linkage with twisted molecular conformation between phenylcarbazole and triazole, for which this conformation significantly impedes the carrier hopping and, in turn, gives reduced mobilities. For all OLEDs, the higher efficiency was achieved for the m-cbtz based device with maximum η_{ext} of 8.8%, 16.7%, 17.5% and 16.7% for blue (FIRpic), green [(ppy)₂Ir(acac)], yellow [(Bt)₂Ir(acac)], and red [Os(bpftz)₂(PPhMe)₂, OS1], respectively. A two-emitter, all phosphorescent WOLED hosted by m-cbtz in a single-emitting layer gave a maximum η_{ext} of 12.4% and with high chromatic stability. Thus, the present study presents an effective molecular design for bipolar hosts of all type of PhOLEDs.

Experimental

Synthesis

Synthesis of 9-(4-bromophenyl)carbazole. A mixture of carbazole (5.0 g, 30 mmol), 1,4-dibromobenzene (10.62 g, 45 mmol), 1,10-phenanthroline (1.62 g, 9 mmol), K₂CO₃ (12.4 g, 90 mmol) and CuI (0.86 g, 5 mmol) was dissolved in DMSO (60 mL) under nitrogen. The mixture was heated to 140 °C slowly and stirred overnight. After cooling to room temperature, solvent was removed by distillation at reduced pressure. Ethyl acetate (250 mL) was added to the residue and then filtered. The filtrate was washed with deionized water three times, dried over Na₂SO₄ and concentrated to dryness. The residue was then purified by column chromatography, eluting with a 1 : 10 mixture of CH₂Cl₂ and hexane to give the product. The colorless crystals were crystallized from a mixture of ethyl acetate and hexane (5.1 g, 15.8 mmol, 52.8%).

Spectral data of 9-(4-bromophenyl)carbazole. ¹H NMR (400 MHz, CDCl₃): δ 8.15 (d, *J* = 7.8 Hz, 2H), 7.73 (d, *J* = 6.4 Hz, 2H), 7.46–7.33 (m, 6H), 7.30 (t, *J* = 5.6 Hz, 2H). ¹³C NMR (100 MHz, CDCl₃): δ 63.55, 59.74, 56.06, 51.65, 49.04, 46.44, 43.82, 43.35, 43.18, 32.50.

Synthesis of p-cbtz. A mixture of 9-(4-bromophenyl)carbazole (1.58 g, 4.3 mmol), 3,5-bis(2-pyridyl)-1*H*-1,2,4-triazole (0.8 g, 3.6 mmol), K₂CO₃ (1.52 g, 10.8 mmol) and CuI (0.14 g, 0.8 mmol) was dissolved in DMF (65 mL) under nitrogen. The mixture was heated to reflux for 36 h. After cooling to room temperature, solvent was removed by distillation at reduced pressure. The

residue was dissolved in 150 mL of CH₂Cl₂ and the solution was filtered. The filtrate was washed with deionized water three times, dried over Na₂SO₄ and concentrated to dryness. The resulting solid was purified by column chromatography, eluting with a 1 : 1 mixture of CH₂Cl₂ and ethyl acetate. The colorless crystals were crystallized from a mixture of CH₂Cl₂ and hexane (0.92 g, 1.98 mmol, 54.9%).

Spectral data of p-cbtz. MS (FAB): *m/z* = 466 (M + 1)⁺, 465 (M⁺). ¹H NMR (400 MHz, CDCl₃): δ 8.83 (d, *J* = 4.4 Hz, 1H), 8.54 (d, *J* = 4.8 Hz, 1H), 8.33 (d, *J* = 8.0 Hz, 1H), 8.27 (d, *J* = 8.0 Hz, 1H), 8.14 (d, *J* = 8.0 Hz, 2H), 7.87 (t, *J* = 8.0 Hz, 2H), 7.73 (d, *J* = 6.4 Hz, 2H), 7.64 (d, *J* = 6.8 Hz, 2H), 7.47–7.36 (m, 6H), 7.30 (t, *J* = 7.2 Hz, 2H). ¹³C NMR (100 MHz, CDCl₃): δ 161.55, 153.83, 150.16, 149.38, 149.22, 147.20, 140.58, 137.97, 137.70, 136.97, 136.83, 127.34, 127.10, 126.12, 124.77, 124.69, 124.18, 123.57, 121.99, 120.40, 120.29, 109.65. Anal. Calcd for C₃₀H₂₀N₆: C, 77.57; H, 4.34; N, 18.09; found: C, 77.90; H, 4.47; N, 18.36%.

Synthesis of 9-(3-iodophenyl)carbazole. Carbazole (1.0 g, 6.0 mmol) and 1,3-diiodobenzene (2.96 g, 9.0 mmol) were reacted according to the general procedure documented for 9-(4-bromophenyl)-9*H*-carbazole, giving 9-(3-iodophenyl)-9*H*-carbazole as colorless solid (0.87 g, 2.1 mmol, 39%).

Spectral data of 9-(3-iodophenyl)carbazole. ¹H NMR (400 MHz, CDCl₃): δ 8.12 (d, *J* = 8.0 Hz, 2H), 7.92 (t, *J* = 2.0 Hz, 1H), 7.79 (d, *J* = 7.6 Hz, 1H), 7.55 (d, *J* = 8.6 Hz, 1H), 7.43–7.37 (m, 4H), 7.34–7.26 (m, 3H). ¹³C NMR (100 MHz, CDCl₃): δ 140.54, 138.95, 136.42, 135.96, 131.23, 126.40, 126.09, 123.48, 120.36, 120.28, 109.58, 94.56.

Synthesis of m-cbtz. 9-(3-Iodobenzene)carbazole (1.2 g, 3.3 mmol) and 3,5-bis(2-pyridyl)-1*H*-1,2,4-triazole (0.6 g, 2.7 mmol) were reacted according to the previous procedure, giving m-cbtz as colorless solid (0.66 g, 1.42 mmol, 52.4%).

Spectral data of m-cbtz. MS (FAB): *m/z* = 465 (M⁺). ¹H NMR (400 MHz, CDCl₃): δ 8.81 (s, 1H), 8.58 (d, *J* = 4.4 Hz, 1H), 8.31–8.26 (m, 2H), 8.09 (d, *J* = 7.6 Hz, 2H), 7.89–7.84 (m, 2H), 7.73–7.71 (m, 2H), 7.66–7.63 (m, 1H), 7.60 (s, 1H), 7.40–7.37 (m, 2H), 7.34–7.31 (m, 4H), 7.28–7.25 (m, 2H). ¹³C NMR (100 MHz, CDCl₃): δ 161.53, 153.79, 150.09, 149.30, 149.24, 147.24, 140.59, 140.46, 137.91, 137.04, 136.77, 130.33, 127.25, 125.93, 124.93, 124.82, 124.68, 124.65, 124.14, 123.41, 121.95, 120.30, 120.18, 109.58. Anal. Calcd for C₃₀H₂₀N₆: C, 77.57; H, 4.34; N, 18.09; found: C, 77.65; H, 4.47; N, 18.30%.

General procedures

All reactions were performed under nitrogen atmosphere and solvents were distilled from appropriate drying agents prior to use. Commercially available reagents were used without further purification unless otherwise stated. All synthetic reactions were monitored using pre-coated TLC plates 0.20 mm with fluorescent indicator UV254. UV-vis and emission spectra were measured on Hitachi U-3900 and F-4500 FL spectrophotometers, respectively. The experimental values of HOMO levels were determined

with a Riken AC-2 photoemission spectrometer (PES), and those of LUMO levels were estimated by subtracting the optical energy gap from the measured HOMO. Differential scanning calorimetry (DSC) was characterized with a TA DSC Q200 at a heating rate of $10\text{ }^{\circ}\text{C min}^{-1}$ from 20 to $250\text{ }^{\circ}\text{C}$ under nitrogen. The glass transition temperature (T_g) was determined from the second heating scan. Thermogravimetric analysis (TGA) was measured with a Perkin-Elmer Pyris 1 TGA instrument. Mass spectra were obtained on a JEOL SX-102A instrument operating in electron impact (EI) or fast atom bombardment (FAB) mode. ^1H NMR spectra were recorded on a Varian Mercury-400 or an INOVA-500 instrument. Elemental analysis was carried out with a Heraeus CHN-O Rapid Elementary Analyzer. Cyclic voltammetry was performed in CH_2Cl_2 solution on a CH1621A instrument with a scan rate of 100 mV s^{-1} . Tetrabutylammonium hexafluorophosphate (TBAPF_6 , 0.1 M) was used as supporting electrolyte. The three electrode cell was used with Pt wire as working electrode, glassy carbon as counter electrode. An Ag/Ag^+ electrode was used as reference electrode with ferrocenium-ferrocene (Fc^+/Fc) as internal standard. 3,5-Bis(2-pyridyl)-1H-1,2,4-triazole (Hbpytz) was synthesized according to the literature procedure.²⁹

Time-of-flight (TOF) mobility measurements

Carrier-transport properties were studied in vapor-deposited glasses of p-cbtz or m-cbtz by the time-of-flight (TOF) transient photocurrent technique. The samples were prepared by vacuum deposition using the structure: ITO glass/p-cbtz ($1.11\text{ }\mu\text{m}$) or m-cbtz ($1.51\text{ }\mu\text{m}$)/Ag (150 nm), and then placed inside a cryostat and kept under vacuum. The thickness of organic film was monitored *in situ* with a quartz sensor and calibrated by a thin film thickness measurement (K-MAC ST2000). A pulsed nitrogen laser was used as the excitation light source through the transparent electrode (ITO) induced photogeneration of a thin sheet of excess carriers. Under an applied dc bias, the transient photocurrent was swept across the bulk of the organic film toward the collection electrode (Ag), and then recorded with a digital storage oscilloscope. Depending on the polarity of the applied bias, selected carriers (holes or electrons) are swept across the sample with a transit time of t_T . With the applied bias V and the sample thickness D , the applied electric field E is V/D , and the carrier mobility is then given by $\mu = D/(t_T E) = D^2/(V t_T)$, in which the carrier transit time, t_T , can be extracted from the intersection of two asymptotes to the tail and plateau sections in double-logarithmic plots.

OLED device fabrications

All chemicals were purified through vacuum sublimation prior to use. The OLEDs were fabricated through vacuum deposition of the materials at 10^{-6} Torr onto ITO-coated glass substrates having a sheet resistance of $15\text{ }\Omega\text{ sq}^{-1}$. The ITO surface was cleaned ultrasonically; *i.e.* with acetone, methanol, and deionized water in sequence, and finally with UV-ozone. The deposition rate of each organic material was *ca.* $1\text{--}2\text{ }\text{\AA}\text{ s}^{-1}$. Subsequently, LiF was deposited at $0.1\text{ }\text{\AA}\text{ s}^{-1}$ and then capped with Al (*ca.* $5\text{ }\text{\AA}\text{ s}^{-1}$) through shadow masking without breaking the vacuum. The $J\text{--}V\text{--}L$ characteristics of the devices were measured

simultaneously in a glove-box using a Keithley 6430 source meter and a Keithley 6487 picoammeter equipped with a calibration Si-photodiode. EL spectra were measured using a photodiode array (OTO SD1200).

Acknowledgements

We are grateful for the financial support from the National Science Council of Taiwan (NSC 100-2112-M-019-002-MY3 and 98-2113-M-007-019-MY3).

Notes and references

- (a) M. A. Baldo, D. F. O'Brien, Y. You, A. Shoustikov, S. Sibley, M. E. Thompson and S. R. Forrest, *Nature*, 1998, **395**, 151; (b) P.-T. Chou and Y. Chi, *Chem.-Eur. J.*, 2007, **13**, 380; (c) Y. Chi and P.-T. Chou, *Chem. Soc. Rev.*, 2010, **39**, 638; (d) L. Xiao, Z. Chen, B. Qu, J. Luo, S. Kong, Q. Gong and J. Kido, *Adv. Mater.*, 2011, **23**, 926.
- (a) Y. Tao, C. Yang and J. Qin, *Chem. Soc. Rev.*, 2011, **40**, 2943; (b) A. Chaskar, H.-F. Chen and K.-T. Wong, *Adv. Mater.*, 2011, **23**, 3876.
- (a) Y. Tao, Q. Wang, C. Yang, Q. Wang, Z. Zhang, T. Zou, J. Qin and D. Ma, *Angew. Chem., Int. Ed.*, 2008, **47**, 8104; (b) Y. Tao, Q. Wang, L. Ao, C. Zhong, J. Qin, C. Yang and D. Ma, *J. Mater. Chem.*, 2010, **20**, 1759; (c) Y. Tao, Q. Wang, Y. Shang, C. Yang, L. Ao, J. Qin, D. Ma and Z. Shuai, *Chem. Commun.*, 2009, 77; (d) Y. Tao, Q. Wang, L. Ao, C. Zhong, C. Yang, J. Qin and D. Ma, *J. Phys. Chem. C*, 2010, **114**, 601.
- (a) F.-M. Hsu, C.-H. Chien, C.-F. Shu, C.-H. Lai, C.-C. Hsieh, K.-W. Wang and P.-T. Chou, *Adv. Funct. Mater.*, 2009, **19**, 2834; (b) S. O. Jeon, K. S. Yook, C. W. Joo and J. Y. Lee, *Adv. Funct. Mater.*, 2009, **19**, 3644; (c) S. Gong, Y. Chen, J. Luo, C. Yang, C. Zhong, J. Qin and D. Ma, *Adv. Funct. Mater.*, 2011, **21**, 1168.
- (a) M. Guan, Z. Chen, Z. Bian, Z. Liu, Z. Gong, W. Baik, H. Lee and C. Huang, *Org. Electron.*, 2006, **7**, 330; (b) L. Zeng, T. Y.-H. Lee, P. B. Merkel and S. H. Chen, *J. Mater. Chem.*, 2009, **19**, 8772.
- L. S. Sapochak, A. B. Padmaperuma, X. Cai, J. L. Male and P. E. Burrows, *J. Phys. Chem. C*, 2008, **112**, 7989.
- C.-H. Chen, W.-S. Huang, M.-Y. Lai, W.-C. Tsao, J. T. Lin, Y.-H. Wu, T.-H. Ke, L.-Y. Chen and C.-C. Wu, *Adv. Funct. Mater.*, 2009, **19**, 2661.
- J. H. Kim, D. Y. Yoon, J. W. Kim and J.-J. Kim, *Synth. Met.*, 2007, **157**, 743.
- (a) J. Kido, C. Ohtaki, K. Hongawa, K. Okuyama and K. Nagai, *Jpn. J. Appl. Phys.*, 1993, **32**, L917; (b) C. Adachi, M. A. Baldo and S. R. Forrest, *Appl. Phys. Lett.*, 2000, **77**, 904; (c) M. Ichikawa, S. Fujimoto, Y. Miyazawa, T. Koyama, N. Yokoyama, T. Miki and Y. Taniguchi, *Org. Electron.*, 2008, **9**, 77; (d) H. Gao, H. Zhang, R. Mo, S. Sun, Z.-M. Su and Y. Wang, *Synth. Met.*, 2009, **159**, 1767; (e) C.-S. Wu and Y. Chen, *J. Polym. Sci., Part A: Polym. Chem.*, 2011, **49**, 3928.
- (a) G. Zhou, W.-Y. Wong and S. Suo, *J. Photochem. Photobiol., C*, 2010, **11**, 133; (b) Q. Wang and D. Ma, *Chem. Soc. Rev.*, 2010, **39**, 2387; (c) K. T. Kamtekar, A. P. Monkman and M. R. Bryce, *Adv. Mater.*, 2010, **22**, 572; (d) M. C. Gather, A. Koehnen and K. Meerholz, *Adv. Mater.*, 2011, **23**, 233; (e) G. M. Farinola and R. Ragni, *Chem. Soc. Rev.*, 2011, **40**, 3467; (f) G. Zhou, W.-Y. Wong and X. Yang, *Chem.-Asian J.*, 2011, **6**, 1706.
- (a) S.-J. Su, H. Sasabe, T. Takeda and J. Kido, *Chem. Mater.*, 2008, **20**, 1691; (b) W.-Y. Lai, Q.-Y. He, D.-Y. Chen and W. Huang, *Chem. Lett.*, 2008, **37**, 986.
- Y. Shirota, *J. Mater. Chem.*, 2000, **10**, 1.
- R. J. Holmes, S. R. Forrest, Y.-J. Tung, R. C. Kwong, J. J. Brown, S. Garon and M. E. Thompson, *Appl. Phys. Lett.*, 2003, **82**, 2422.
- M. Borsenberger, D. S. Weiss, in *Organic Photoreceptors for Imaging Systems*, New York 1993, and references therein.
- S.-J. Su, T. Chiba, T. Takeda and J. Kido, *Adv. Mater.*, 2008, **20**, 2125.

- 16 A. F. Rausch, M. E. Thompson and H. Yersin, *J. Phys. Chem. A*, 2009, **113**, 5927.
- 17 C. Adachi, M. A. Baldo, M. E. Thompson and S. R. Forrest, *J. Appl. Phys.*, 2001, **90**, 5048.
- 18 S.-J. Su, H. Sasabe, T. Takeda and J. Kido, *Chem. Mater.*, 2008, **20**, 1691.
- 19 Y.-L. Tung, S.-W. Lee, Y. Chi, Y.-T. Tao, C.-H. Chien, Y.-M. Cheng, P.-T. Chou, S.-M. Peng and C.-S. Liu, *J. Mater. Chem.*, 2005, **15**, 460.
- 20 D.-H. Lee, Y.-P. Liu, K.-H. Lee, H. Chae and S. M. Cho, *Org. Electron.*, 2010, **11**, 427.
- 21 (a) S.-J. Su, E. Gonmori, H. Sasabe and J. Kido, *Adv. Mater.*, 2008, **20**, 4189; (b) Y.-Y. Lyu, J. Kwak, W. S. Jeon, Y. Byun, H. S. Lee, D. Kim, C. Lee and K. Char, *Adv. Funct. Mater.*, 2009, **19**, 420.
- 22 L. Xiao, S.-J. Su, Y. Agata, H. Lan and J. Kido, *Adv. Mater.*, 2009, **21**, 1271.
- 23 M.-H. Tsai, H.-W. Lin, H.-C. Su, T.-H. Ke, C.-C. Wu, F.-C. Fang, Y.-L. Liao, K.-T. Wong and C.-L. Wu, *Adv. Mater.*, 2006, **18**, 1216.
- 24 W.-Y. Hung, Z.-W. Chen, H.-W. You, F.-C. Fan, H.-F. Chen and K.-T. Wong, *Org. Electron.*, 2011, **12**, 575.
- 25 H.-H. Chou and C.-H. Cheng, *Adv. Mater.*, 2010, **22**, 2468.
- 26 (a) C.-L. Ho, W.-Y. Wong, Q. Wang, D. Ma, L. Wang and Z. Lin, *Adv. Funct. Mater.*, 2008, **18**, 928; (b) Y.-S. Park, J.-W. Kang, D. M. Kang, J.-W. Park, Y.-H. Kim, S.-K. Kwon and J.-J. Kim, *Adv. Mater.*, 2008, **20**, 1957; (c) W.-Y. Hung, L.-C. Chi, W.-J. Chen, Y.-M. Chen, S.-H. Chou and K.-T. Wong, *J. Mater. Chem.*, 2010, **20**, 10113; (d) S.-L. Lai, S.-L. Tao, M.-Y. Chan, M.-F. Lo, T.-W. Ng, S.-T. Lee, W.-M. Zhao and C.-S. Lee, *J. Mater. Chem.*, 2011, **21**, 4983; (e) R. Wang, D. Liu, H. Ren, T. Zhang, H. Yin, G. Liu and J. Li, *Adv. Mater.*, 2011, **23**, 2823.
- 27 H. Sasabe, J. Takamatsu, T. Motoyama, S. Watanabe, G. Wagenblast, N. Langer, O. Molt, E. Fuchs, C. Lennartz and J. Kido, *Adv. Mater.*, 2010, **22**, 5003.
- 28 (a) Y.-H. Niu, Y.-L. Tung, Y. Chi, C.-F. Shu, J. H. Kim, B. Chen, J. Luo, A. J. Carty and A. K.-Y. Jen, *Chem. Mater.*, 2005, **17**, 3532; (b) Y. Zhang, F. Huang, Y. Chi and A. K.-Y. Jen, *Adv. Mater.*, 2008, **20**, 1565; (c) C.-H. Chien, S.-F. Liao, C.-H. Wu, C.-F. Shu, S.-Y. Chang, Y. Chi, P.-T. Chou and C.-H. Lai, *Adv. Funct. Mater.*, 2008, **18**, 1430.
- 29 H. Takalo, V.-M. Mikkala and L. Meriö, *Helv. Chim. Acta*, 1997, **80**, 372.